Analysis of Regenerative Chatter in Tandem Cold Rolling Mills

(Article begins on next page)

Accepted version. Version of record available: A. Floris, R. Galluzzi, and N. Amati, “Analysis of Regenerative Chatter in Tandem Cold Rolling Mills,” J. Manuf. Sci. Eng, vol. 148, no. 091008, Jul. 2026, doi: 10.1115/1.4072226.
https://doi.org/10.1115/1.4072226

Analysis of Regenerative Chatter in Tandem Cold Rolling Mills

Andrea Floris
Department of Mechanical and Aerospace Engineering,
Politecnico di Torino,
Corso Duca degli Abruzzi 24,
10129 Turin, Italy
email: andrea.floris@polito.it

Renato Galluzzi[1]
School of Engineering and Sciences,
Tecnologico de Monterrey,
Calle del Puente 222,
14380 Mexico City, Mexico
email: renato.galluzzi@tec.mx

Nicola Amati
Department of Mechanical and Aerospace Engineering,
Politecnico di Torino,
Corso Duca degli Abruzzi 24,
10129 Turin, Italy
email: nicola.amati@polito.it

Regenerative chatter in tandem cold rolling mills poses a significant challenge to process stability and productivity, arising from complex interactions between process dynamics and structural vibrations. In this paper a novel stability criterion for regenerative chatter based on linear analysis tools is introduced, offering a more precise and computationally efficient alternative to other methods present in the literature to compute the critical speed starting from a linear chatter model. The criterion serves as the foundation for generating multi-parametric stability charts that provide valuable insights into the underlying phenomena and help clarify discrepancies reported in previous studies. Furthermore, an innovative parameterization is introduced to investigate the effects on regenerative chatter of structural modifications on the stands, revealing that aligning the resonance of the downstream stand with the anti-resonance of the upstream stand substantially enhances system stability. The proposed tool enables the evaluation of stability over a fine parameter grid within minutes, while previous approaches yield results after multiple computational hours.

Keywords: tandem cold rolling, chatter, regenerative chatter, negative damping, stability analysis, stability criterion, process optimization

1 Introduction

Cold rolling is a metalworking process that yields high-volume strips, but has long been plagued by self-excited vibrational issues. These phenomena, collectively termed chatter, degrade the surface finish, induce thickness variations, and force unplanned slow-downs [1,2]. Given the high capital investment required for the construction of such machinery, maximizing productivity and preventing unplanned slowdowns is of great interest, as they significantly impact the cost of the final product [3]. Extensive research efforts [4] have resulted in the classification of chatter phenomena into three principal categories: third-octave, fifth-octave, and torsional chatter. Specifically, the third-octave mode is the most serious chatter type [5–7], as it leads to severe gauge variation and, in severe cases, to strip rupture or even mechanical damage to the rolling mill.

As pointed out in various studies [8–11], third-octave-mode chatter can be generated by means of model matching, negative damping, mode coupling, and regeneration effects. These mechanisms are all self-excited in nature, but they differ in the physical feedback path through which mechanical energy is supplied to the vibration. Negative-damping chatter arises when the process related to mill vibration induces further vibrations, thus amplifying oscillations rather than dissipating them. In this case, stand vibration yields variations in the roll-gap height, which, in turn, generate rolling-force perturbations containing a component in phase with the vibration velocity. As a result, the rolling process performs positive work over a vibration cycle and behaves as a negative equivalent damping acting on the chatter structural mode. This effect was first illustrated by Tamiya et al. [1] and Tlusty et al. [2], and later captured in a homogeneous process–structure model by Hu et al. [12]. In contrast, mode-coupling chatter takes place through the interaction of two structural vibration modes (e.g. horizontal and vertical roll motions), thereby creating new instability regions. Here, the rolling process couples the two modal coordinates: the motion associated with one mode modifies the roll-gap, contact conditions, or rolling force, and the resulting force perturbation excites the other mode. Instability may therefore occur even if each mode would be stable when considered separately, because energy is transferred between the coupled modes through the process dynamics. Yun [13] and Yun et al. [14] first introduced this analogy from metal cutting. Later, Hu and Ehmann embedded it within a full transfer-matrix framework [15]. Model-matching chatter is a more subtle instability associated with the closed-loop coupling between the rolling-process model and the mill-structure model. Even when the isolated process and structural subsystems are stable, their dynamic interaction can generate destabilizing equivalent stiffness and damping contributions if their frequency responses are poorly matched. In this sense, model matching is a system-level process–structure instability. It can be difficult to detect in reduced input-output representations because pole-zero cancellations may hide relevant internal dynamics in play [8]. Finally, regenerative chatter in rolling occurs when surface ripples left by one stand modulate the entry thickness to the next, hence creating a self-exciting feedback loop. Unlike the previous mechanisms, regeneration is intrinsically related to the memory of the strip surface and to the transport of thickness undulations between consecutive stands. A vibration in an upstream or downstream stand leaves a periodic thickness imprint on the strip. After a finite transport time, this waviness modifies the entry thickness and rolling force of a neighboring stand. The resulting force fluctuation can then generate new surface waviness, closing a delayed feedback loop. In contrast to single-stand mechanisms, regenerative chatter requires at least two consecutive stands because the feedback loop is closed by the transport of strip waviness from one stand to another. Given their relevance to the scope of the present work, and because negative damping represents one of the most direct mechanisms of instability [16], negative-damping and regenerative chatter mechanisms are schematized in Fig. 1. Chefneux et al. were among the first to recognize that chatter in a tandem mill arises not only from each stand individually but also from the way successive stands interact [17]. They described two coupling pathways: (i) a delayed interaction, in which the thickness profile leaving one stand re-enters the next after a transit delay; and (ii) an

[1]Corresponding Author.
Version: June 15, 2026

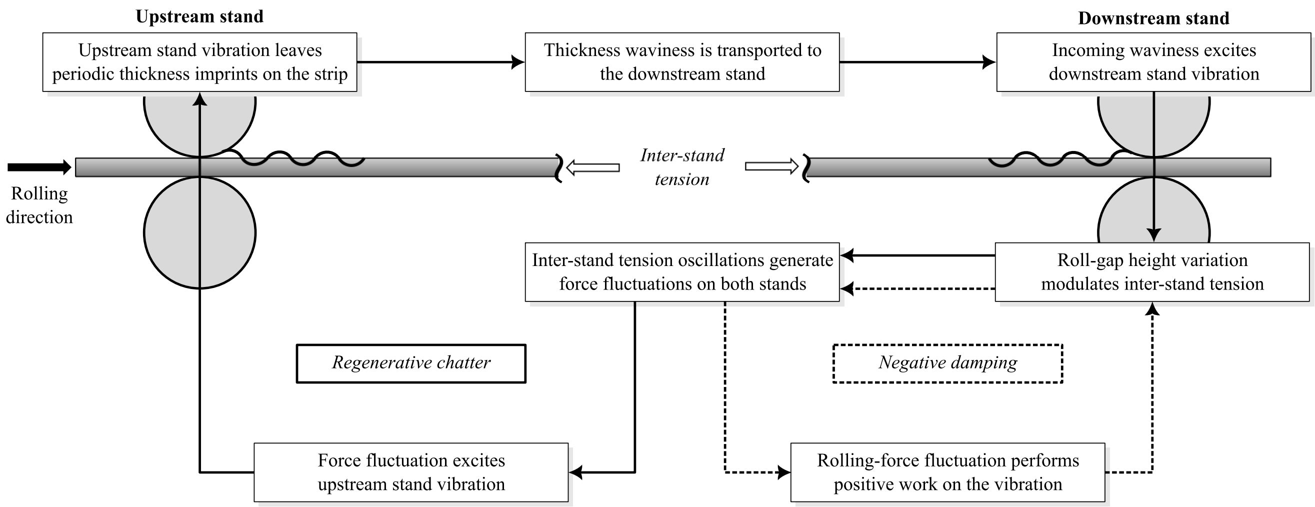

Figure 1 Schematic representation of the negative-damping and regenerative chatter mechanisms. Dashed arrows indicate the local energy-feeding path associated with negative damping, whereas solid arrows indicate the delayed regenerative path mediated by transported strip waviness. For clarity, only the interaction between two consecutive stands is shown. The upstream stand may also experience its own negative-damping mechanism, and the downstream stand may, in turn, interact regeneratively with the following stand.

immediate interaction, where any change in strip velocity instantly alters the inter-stand tension. Yun embraced the idea of regeneration from machining—where surface waviness left by a cutting tool re-excites the tool on its next pass—but pointed out that a direct analogy fails in rolling, since the roll does not re-contact the same material point [13]. Thus, in rolling, the regenerative effect should not be interpreted as the same material point being cut or rolled again, but rather as a stand-to-stand feedback mechanism mediated by transported strip waviness and inter-stand tension dynamics.

Experimental evidence consistently points to the regenerative mechanism as the dominant cause of third-octave instability in actual tandem mills. In situ measurements on production stands have repeatedly revealed the characteristic wave-pulse modulation and single, narrow-band spectral peak—typically within the 100–250 Hz range—that mark a self-excited regenerative process. Niroomand et al. documented these features in a series of full-scale investigations [16,18–20], where accelerometer and acoustic recordings showed coherent third-octave components propagating along consecutive stands with delays matching the strip transport time. Such delayed correlation is incompatible with pure single-stand negative-damping models and instead confirms the presence of a feedback loop through the strip. Consequently, while traditional models have emphasized local instability mechanisms, plant data indicate that regenerative chatter governs the onset and evolution of third-octave vibrations, effectively setting the practical stability limit for high-speed tandem cold rolling.

Formulating an effective stability criterion for the regenerative effect, and in particular for the delayed interaction, has been proved nontrivial. Moreover, the influence of various operating parameters on the rolling process remains unclear to date [21]. In fact, the work by Yun [13] did not explore how the finite transport delay itself affects stability, choosing instead to treat the mill as a whole. Another attempt to investigate stability of tandem mills with the regenerative effect was made by Hu et al. [7], but again the transport delay term was neglected to use classic root locus techniques for stability analysis. The first actual attempt to evaluate stability of a rolling tandem with delayed interaction was carried out by Zhao and Ehmann [21]. They employed an integral approach based on the stability of delay differential equations. Despite the valuable insights provided by their method, the integral approach is computationally intensive. Regenerative chatter remains a loosely sketched concept without a unified dynamic model or concise design rules. This gap prevents practitioners from predicting regenerative thresholds or designing targeted dampers for modern high-speed, multi-stand mills. Because regenerative chatter is arguably the most critical instability in cold rolling, a more efficient tool is essential to develop reliable mitigation strategies.

The aim of this work is to introduce a novel stability criterion for regenerative chatter in tandem cold rolling mills. The proposed approach separates the delay-free local interaction between neighboring stands from the strip-transport delay, which is treated separately as the mechanism closing the regenerative feedback loop. This enables the use of standard frequency-domain linear analysis tools while retaining the physical meaning of the delayed regenerative mechanism. In addition, we present a case study of the regenerative mechanism and explore its relationship with some of the most critical process parameters. Moreover, this work makes, for the first time, a structured attempt to clarify how mill design choices influence susceptibility to regenerative chatter.

The paper is structured as follows. First, a general mathematical model capable of capturing regenerative chatter phenomena is developed from first principles. It has the goal of summarizing and clarifying the distinct interactions between the process dynamics, single-stand behavior, and the coupling mechanisms that arise in a tandem configuration——all of which can contribute to system instability. Next, the proposed stability criterion is presented and its predictive accuracy is evaluated by comparing its results against detailed time-domain simulations. Finally, the criterion is employed in a parametric stability analysis, focusing on variations of the friction coefficient and structural modifications to the mill. This last step leads to meaningful insights for chatter-resistant design strategies.

The subject of process or structure modeling strategies is beyond the scope of this paper. To best contextualize our work within the current state of the art, the results herein are benchmarked against the model and data employed by Zhao and Ehmann [21]. Nevertheless, the proposed criterion is designed with general applicability in mind, ensuring adaptability and usage across a broad range of scenarios beyond the specific case considered here.

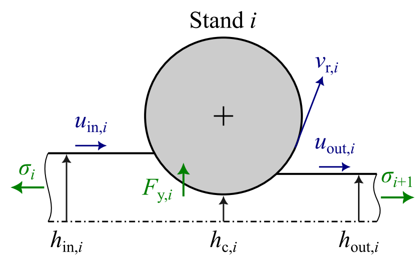

Figure 2 Rolling process schematization for the ith stand. $h_{\mathrm{in},i}$ and $h_{\mathrm{out},i}$ are entry and exit strip thicknesses, $u_{\mathrm{in},i}$ and $u_{\mathrm{out},i}$ are the entry and exit strip speeds, σ_i and σ_{i+1} are the upstream and downstream strip horizontal stresses, $h_{\mathrm{c},i}$ is the minimum gap height, $v_{\mathrm{r},i}$ is the work roll peripheral speed, $F_{\mathrm{y},i}$ is the vertical rolling resultant force.

2 Chatter model

A chatter model is a mathematical representation capable of capturing the onset and evolution of chatter phenomena. Such a model is composed of mechanical states, which describe the structural dynamics of the stand, and process-related states, which characterize the rolling operation itself.

In the following sections, the development of the chatter model is presented in a structured manner. First, the model describing the rolling process in isolation is introduced. Subsequently, the coupling between the rolling process and the structural dynamics of a single stand is detailed. Finally, the interaction among multiple stands operating in tandem configurations is addressed, highlighting the mechanisms by which instability may propagate throughout the mill.

2.1 Process model. Process models are often quite complex and of nonlinear form and can be derived using several modeling techniques and assumptions. Generally, the ith vertical rolling bite model takes the boundary inter-stand stress values σ_i and σ_{i+1} as inputs, the gap height and its rate of change $h_{\mathrm{c},i}$ and $\dot{h}_{\mathrm{c},i}$, and the entry thickness $h_{\mathrm{in},i}$. Conversely, it yields the following outputs: entry and exit speeds $u_{\mathrm{in},i}$ and $u_{\mathrm{out},i}$, rolling force $F_{\mathrm{y},i}$ and exit thickness $h_{\mathrm{out},i}$ (see Fig. 2). For the latter, it is usually convenient to assume its value equal to the gap height $h_{\mathrm{c},i}$. This assumption corresponds to neglecting elastic recovery and other local thickness corrections at the roll exit, so that small variations of exit thickness are directly related to small variations of the minimum roll gap. In compact form, the nonlinear rolling-bite relation for the ith stand can be expressed as

$$\begin{bmatrix} u_{\mathrm{in},i} \\ u_{\mathrm{out},i} \\ F_{\mathrm{y},i} \\ h_{\mathrm{out},i} \end{bmatrix} = \mathbf{\Phi}_i \left(h_{\mathrm{c},i}, \dot{h}_{\mathrm{c},i}, \sigma_i, \sigma_{i+1}, h_{\mathrm{in},i}; R_i, \mu_i, v_{\mathrm{r},i}, \mathbf{p}_{\mathrm{mat},i} \right), \tag{1}$$

where $\mathbf{\Phi}_i(\cdot)$ denotes the generic nonlinear process function associated with the selected rolling model. The variables before the semicolon are the process quantities retained as dynamic inputs of the local bite model. The quantities after the semicolon are operating or technological parameters defining the steady rolling condition: R_i is the work-roll radius, μ_i is the strip–roll friction coefficient, $v_{\mathrm{r},i}$ is the work-roll peripheral speed, and $\mathbf{p}_{\mathrm{mat},i}$ collects the material parameters required by the selected rolling law, such as the flow-stress model and elastic properties.

For stability analysis purposes, it is common to derive a linearized form of the process model, resulting in a matrix of coefficients relating each one of the inputs to each one of the outputs:

$$\begin{bmatrix} du_{\mathrm{in},i} \\ du_{\mathrm{out},i} \\ dF_{\mathrm{y},i} \\ dh_{\mathrm{out},i} \end{bmatrix} = \begin{bmatrix} P_1 & P_2 & P_3 & P_4 & P_5 \\ Q_1 & Q_2 & Q_3 & Q_4 & Q_5 \\ F_1 & F_2 & F_3 & F_4 & F_5 \\ 1 & 0 & 0 & 0 & 0 \end{bmatrix}_i \begin{bmatrix} dh_{\mathrm{c},i} \\ d\dot{h}_{\mathrm{c},i} \\ d\sigma_i \\ d\sigma_{i+1} \\ dh_{\mathrm{in},i} \end{bmatrix} = \left.\begin{bmatrix} \frac{\partial u_{\mathrm{in},i}}{\partial h_{\mathrm{c},i}} & \frac{\partial u_{\mathrm{in},i}}{\partial \dot{h}_{\mathrm{c},i}} & \frac{\partial u_{\mathrm{in},i}}{\partial \sigma_i} & \frac{\partial u_{\mathrm{in},i}}{\partial \sigma_{i+1}} & \frac{\partial u_{\mathrm{in},i}}{\partial h_{\mathrm{in},i}} \\ \frac{\partial u_{\mathrm{out},i}}{\partial h_{\mathrm{c},i}} & \frac{\partial u_{\mathrm{out},i}}{\partial \dot{h}_{\mathrm{c},i}} & \frac{\partial u_{\mathrm{out},i}}{\partial \sigma_i} & \frac{\partial u_{\mathrm{out},i}}{\partial \sigma_{i+1}} & \frac{\partial u_{\mathrm{out},i}}{\partial h_{\mathrm{in},i}} \\ \frac{\partial F_{\mathrm{y},i}}{\partial h_{\mathrm{c},i}} & \frac{\partial F_{\mathrm{y},i}}{\partial \dot{h}_{\mathrm{c},i}} & \frac{\partial F_{\mathrm{y},i}}{\partial \sigma_i} & \frac{\partial F_{\mathrm{y},i}}{\partial \sigma_{i+1}} & \frac{\partial F_{\mathrm{y},i}}{\partial h_{\mathrm{in},i}} \\ 1 & 0 & 0 & 0 & 0 \end{bmatrix}\right|_{\mathrm{op}} \begin{bmatrix} dh_{\mathrm{c},i} \\ d\dot{h}_{\mathrm{c},i} \\ d\sigma_i \\ d\sigma_{i+1} \\ dh_{\mathrm{in},i} \end{bmatrix} \tag{2}$$

These coefficients correspond to the local partial derivatives of the nonlinear process function evaluated at the steady rolling condition (op). Thus, the P_i coefficients are the local sensitivities of the entry speed, the Q_i coefficients are the local sensitivities of the exit speed, and the F_i coefficients are the local sensitivities of the vertical rolling force with respect to the five dynamic process inputs. The linearization is performed with respect to $h_{\mathrm{c},i}$, $\dot{h}_{\mathrm{c},i}$, σ_i, σ_{i+1}, and $h_{\mathrm{in},i}$ because these are the variables through which the rolling bite exchanges perturbations with the stand structure and with the adjacent strip spans. In contrast, R_i, μ_i, $v_{\mathrm{r},i}$, and the material properties are treated as operating parameters that define the steady point around which the dynamic model is linearized. When parameter studies are performed, these quantities are varied from one operating point to another and the coefficients in Eq. (2) are recomputed accordingly. All variables in Eq. (2) denote small perturbations around the steady rolling condition.

In the present formulation, the specific nonlinear rolling model used to compute these coefficients is not the focus. Rather, Eq. (2) is used as a general linear interface between the rolling process and the structural/tension dynamics.

Furthermore, the inter-stand relationship should be set, namely to couple two adjacent stands through the corresponding strip span. The strip spans couple neighboring stands through a delayed interaction, transferring the strip-thickness perturbations between consecutive bites, and through the strip-span stiffness, which relate strip-velocity perturbations to the evolution of inter-stand stress perturbations. To account for the former, a transport-delay operator $e^{-s\Delta_i}$ is usually introduced. The delay Δ_i represents the time required for a thickness perturbation generated at the exit of stand $i-1$ to reach the entry of stand i, and is defined as

$$\Delta_i = \frac{L_i}{u_{\text{out},i-1}} = \frac{L_i}{u_{\text{in},i}}. \tag{3}$$

For the strip-span stiffness model it is common to consider the strip segment between two stands as having an equivalent longitudinal stress stiffness E/L, where E represents the rolled material Young's modulus and L the stand spacing, which is usually constant in a tandem. This relation can be obtained by treating the inter-stand strip span as a lumped longitudinal elastic element; In other words, the inter-stand stress is assumed to be spatially uniform within each span and to respond instantaneously to the velocity mismatch between its two boundaries. Consider the strip segment between two consecutive stands, with undeformed length L and cross-sectional area A. Its incremental axial elongation $d\ell$ produces an average longitudinal strain perturbation

$$d\varepsilon = \frac{d\ell}{L}. \tag{4}$$

Assuming linear elastic behavior of the strip span around the steady operating condition, the corresponding stress perturbation is

$$d\sigma = E\,d\varepsilon = \frac{E}{L}d\ell, \tag{5}$$

thus leading to the time derivative

$$\dot{\sigma} = \frac{E}{L}\dot{\ell}. \tag{6}$$

The elongation rate $\dot{\ell}$ is given by the difference between the velocities imposed at the two ends of the strip span. Therefore, for the upstream span of stand i, $\dot{\ell} = du_{\text{in},i} - du_{\text{out},i-1}$, whereas for the downstream span, $\dot{\ell} = du_{\text{in},i+1} - du_{\text{out},i}$. This leads directly to the stress-evolution law reported in Eq. (7).

$$\dot{\sigma}_i = \frac{E}{L}(du_{\text{in},i} - du_{\text{out},i-1}), \qquad \dot{\sigma}_{i+1} = -\frac{E}{L}(du_{\text{in},i+1} - du_{\text{out},i}). \tag{7}$$

Since the state variable is the strip stress rather than the axial force, the cross-sectional area does not appear explicitly; if force were used instead, the corresponding axial stiffness would be EA/L. As a first approximation, constant boundary strip velocities are imposed, which in the variational formulation means that the perturbations of the velocities imposed by the adjacent stands are set to zero:

$$du_{\text{out},i-1} = 0, \qquad du_{\text{in},i+1} = 0. \tag{8}$$

Hence, the dynamics of the neighboring stands can be excluded from the single-bite process formulation, as they only provide fixed velocity boundaries for the upstream and downstream strip spans. Under this assumption, Eq. (7) is reduced to

$$\begin{bmatrix} \dot{\sigma}_i \\ \dot{\sigma}_{i+1} \end{bmatrix} = \frac{E}{L}\begin{bmatrix} du_{\text{in},i} \\ -du_{\text{out},i} \end{bmatrix} \tag{9}$$

Substituting the corresponding expressions of the entry and exit strip-velocity perturbations, $du_{\text{in},i}$ and $du_{\text{out},i}$, from Eq. (2) into Eq. (9) yields the state-space representation of the single-bite process model. In this formulation, the entry and exit stress perturbations, $d\sigma_i$ and $d\sigma_{i+1}$, are the state variables, while the bite-condition perturbations, $dh_{\text{c},i}$ and $d\dot{h}_{\text{c},i}$, act as inputs. The resulting vertical process-force perturbation, $dF_{\text{y},i}$, is the model output. The final state-space equations are reported in Eq. (10).

$$\begin{cases} \begin{bmatrix} \dot{\sigma}_i \\ \dot{\sigma}_{i+1} \end{bmatrix} = \frac{E}{L}\begin{bmatrix} P_3 & P_4 \\ -Q_3 & -Q_4 \end{bmatrix}_i \begin{bmatrix} d\sigma_i \\ d\sigma_{i+1} \end{bmatrix} + \frac{E}{L}\begin{bmatrix} P_1 & P_2 \\ -Q_1 & -Q_2 \end{bmatrix}_i \begin{bmatrix} dh_{\text{c},i} \\ d\dot{h}_{\text{c},i} \end{bmatrix} + \frac{E}{L}\begin{bmatrix} P_5 \\ -Q_5 \end{bmatrix}_i dh_{\text{in},i} \\ \begin{bmatrix} dF_{\text{y},i} \\ dh_{\text{out},i} \end{bmatrix} = \begin{bmatrix} F_3 & F_4 \\ 0 & 0 \end{bmatrix}_i \begin{bmatrix} d\sigma_i \\ d\sigma_{i+1} \end{bmatrix} + \begin{bmatrix} F_1 & F_2 \\ 1 & 0 \end{bmatrix}_i \begin{bmatrix} dh_{\text{c},i} \\ d\dot{h}_{\text{c},i} \end{bmatrix} + \begin{bmatrix} F_5 \\ 0 \end{bmatrix}_i dh_{\text{in},i} \end{cases} \tag{10}$$

For later use, the linearized process model in Eq. (10) can be rewritten in compact state-space form

$$\begin{cases} \begin{bmatrix} \dot{\sigma}_i \\ \dot{\sigma}_{i+1} \end{bmatrix} = \mathbf{A}_{\text{p},i}\begin{bmatrix} d\sigma_i \\ d\sigma_{i+1} \end{bmatrix} + \mathbf{B}_{\text{p},i}\begin{bmatrix} dh_{\text{c},i} \\ d\dot{h}_{\text{c},i} \end{bmatrix} + \mathbf{G}_{\text{p},i}dh_{\text{in},i}, \\ dF_{\text{y},i} = \mathbf{C}_{\text{p},i}\begin{bmatrix} d\sigma_i \\ d\sigma_{i+1} \end{bmatrix} + \mathbf{D}_{\text{p},i}\begin{bmatrix} dh_{\text{c},i} \\ d\dot{h}_{\text{c},i} \end{bmatrix} + \mathbf{L}_{\text{p},i}dh_{\text{in},i}, \\ dh_{\text{out},i} = \begin{bmatrix} 0 & 0 \end{bmatrix}\begin{bmatrix} d\sigma_i \\ d\sigma_{i+1} \end{bmatrix} + \begin{bmatrix} 1 & 0 \end{bmatrix}\begin{bmatrix} dh_{\text{c},i} \\ d\dot{h}_{\text{c},i} \end{bmatrix} + 0\,dh_{\text{in},i}. \end{cases} \tag{11}$$

In Eq. (11), inputs and outputs are split into more parts to make the subsequent coupling with the stand structural model and the regenerative input–output formulation seamless.

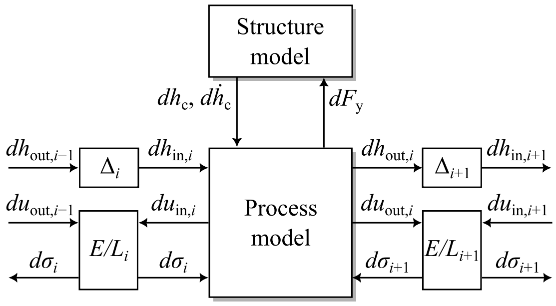

Figure 3 Block diagram of the coupled process–structure model for stand i and its adjacent strip spans. The process model relates the bite-condition perturbations, $dh_{c,i}$ and $d\dot{h}_{c,i}$, and the entry/exit stress perturbations, $d\sigma_i$ and $d\sigma_{i+1}$, to the vertical rolling-force perturbation, $dF_{y,i}$, and to the entry/exit strip-velocity perturbations, $du_{in,i}$ and $du_{out,i}$. The upstream and downstream strip spans couple stand i with the neighboring stands through the transport-delay operator Δ and through the strip-span stiffness model E/L.

2.2 Single stand model. The process interacts with the structure dynamics by accepting the work roll states as inputs and producing the rolling vertical force as output. The complete model of a single-stand is schematized in Fig. 3. A general state-space form for the vertical structural dynamics of the ith stand is introduced in Eq.(12):

$$\begin{cases} \dot{\mathbf{x}}_{s,i} = \mathbf{A}_{s,i}\mathbf{x}_{s,i} + \mathbf{B}_{s,i}\, dF_{y,i}, \\ \begin{bmatrix} dh_{c,i} \\ d\dot{h}_{c,i} \end{bmatrix} = \mathbf{C}_{s,i}\mathbf{x}_{s,i}. \end{cases} \tag{12}$$

where $\mathbf{x}_{s,i}$ is the structural state vector of the vertical stand model, $\mathbf{A}_{s,i}$, $\mathbf{B}_{s,i}$ and $\mathbf{C}_{s,i}$ are the corresponding state-space matrices, and $dF_{y,i}$ is the perturbation of the vertical rolling force acting on the roll stack. The output vector contains the roll-gap perturbation $dh_{c,i}$ and its rate of variation $d\dot{h}_{c,i}$, which are the structural variables supplied to the rolling-process model. The outputs are structural states of the system, therefore, no direct feedthrough term is introduced i.e., $\mathbf{D}_{s,i} = 0$.

By coupling this vertical structural model with the compact process model, a state-space model can be established with the process–structure behavior, entry-thickness perturbation $dh_{in,i}$ as input and exit thickness perturbation $h_{out,i}$ as output:

$$\begin{cases} \begin{bmatrix} \dot{\mathbf{x}}_{s,i} \\ \dot{\sigma}_i \\ \dot{\sigma}_{i+1} \end{bmatrix} = \begin{bmatrix} \mathbf{A}_{s,i} + \mathbf{B}_{s,i}\mathbf{D}_{p,i}\mathbf{C}_{s,i} & \mathbf{B}_{s,i}\mathbf{C}_{p,i} \\ \mathbf{B}_{p,i}\mathbf{C}_{s,i} & \mathbf{A}_{p,i} \end{bmatrix} \begin{bmatrix} \mathbf{x}_{s,i} \\ d\sigma_i \\ d\sigma_{i+1} \end{bmatrix} + \begin{bmatrix} \mathbf{B}_{s,i}\mathbf{L}_{p,i} \\ \mathbf{G}_{p,i} \end{bmatrix} dh_{in,i}, \\ dh_{out,i} = \begin{bmatrix} [1 \;\; 0]\, \mathbf{C}_{s,i} & [0 \;\; 0] \end{bmatrix} \begin{bmatrix} \mathbf{x}_{s,i} \\ d\sigma_i \\ d\sigma_{i+1} \end{bmatrix}. \end{cases} \tag{13}$$

When matched with the structural model, the process is known to affect the stand dynamics following two mechanisms: model matching and negative damping. Mode coupling is not considered here because the structural dynamics is restricted to the vertical direction. In the model-matching mechanism, the rolling process modifies the apparent dynamic properties of the stand through its linearized force sensitivities. In particular, the coefficient F_1, which relates rolling-force perturbations to roll-gap variations, acts as an equivalent process stiffness and shifts the effective stiffness and natural frequency of the vertical chatter mode. More generally, model matching refers to the closed-loop interaction between the process dynamics and the structural dynamics, by which the process-induced stiffness and damping contributions modify the poles of the coupled single-stand system.

In contrast, negative damping is associated with the phase of the rolling-force perturbation relative to the work-roll motion. When fluctuations of the process states, such as inter-stand stresses and strip speeds, generate a force component in phase with the work-roll velocity, the rolling process performs positive work over a vibration cycle. The stand vibration then becomes progressively less damped as rolling speed increases, until the negative process-induced damping exceeds the sum of the positive bite damping and the inherent structural damping of the stand. At this point, the single stand becomes unstable. It must be noted that lower chatter frequencies adversely affect stability. This occurs because forces associated with fluctuations in the process states depend on the gap oscillations in an integral manner—as expressed in Eq. (10)—resulting in amplified inter-stand stress oscillations for longer vibration periods.

2.3 Multi-stand model. The interaction between two consecutive stands in a tandem configuration is characterized by two key features:

- *Shared process state.* The horizontal stress between two stands is influenced by the exit speed of the upstream stand and the entry speed of the downstream stand and affects both stands simultaneously.
- *Chatter marks on the strip.* Vibrations in a stand cause surface undulations, which travel with the strip and excite the downstream stand after a transport delay Δ, directly proportional to the stand spacing L and inversely proportional to the inter-stand strip speed.

The model for a tandem configuration of two or more stands can be schematized as the sequencing of multiple blocks like the one shown in Fig. 3. For a tandem of two stands, the compact process formulation of Eq. (10) can be extended to two neighboring bites by writing the same set of equations for stand $i-1$ and by enforcing the continuity of the inter-stand stress shared by the two bites. In particular, the exit stress state of stand $i-1$, namely $d\sigma_i$, is also the entry stress state of stand i. Therefore, the two single-bite process models can be merged into a single tandem process model with three stress states, $d\sigma_{i-1}$, $d\sigma_i$, and $d\sigma_{i+1}$. The process state space equations for a tandem of two stands $i-1$ and i are in Eq. (14):

$$\begin{cases} \begin{bmatrix} \dot{\sigma}_{i-1} \\ \dot{\sigma}_i \\ \dot{\sigma}_{i+1} \end{bmatrix} = \dfrac{E}{L} \begin{bmatrix} P_{3,i-1} & P_{4,i-1} & 0 \\ -Q_{3,i-1} & -Q_{4,i-1}+P_{3,i} & P_{4,i} \\ 0 & -Q_{3,i} & -Q_{4,i} \end{bmatrix} \begin{bmatrix} d\sigma_{i-1} \\ d\sigma_i \\ d\sigma_{i+1} \end{bmatrix} \\ \qquad + \dfrac{E}{L} \begin{bmatrix} P_{1,i-1} & P_{2,i-1} \\ -Q_{1,i-1} & -Q_{2,i-1} \\ 0 & 0 \end{bmatrix} \begin{bmatrix} dh_{c,i-1} \\ d\dot{h}_{c,i-1} \end{bmatrix} + \dfrac{E}{L} \begin{bmatrix} 0 & 0 \\ P_{1,i} & P_{2,i} \\ -Q_{1,i} & -Q_{2,i} \end{bmatrix} \begin{bmatrix} dh_{c,i} \\ d\dot{h}_{c,i} \end{bmatrix} + \dfrac{E}{L} \begin{bmatrix} 0 \\ P_{5,i} \\ -Q_{5,i} \end{bmatrix} dh_{\text{in},i}, \\ dF_{y,i-1} = \begin{bmatrix} F_{3,i-1} & F_{4,i-1} & 0 \end{bmatrix} \begin{bmatrix} d\sigma_{i-1} \\ d\sigma_i \\ d\sigma_{i+1} \end{bmatrix} + \begin{bmatrix} F_{1,i-1} & F_{2,i-1} \end{bmatrix} \begin{bmatrix} dh_{c,i-1} \\ d\dot{h}_{c,i-1} \end{bmatrix}, \\ dF_{y,i} = \begin{bmatrix} 0 & F_{3,i} & F_{4,i} \end{bmatrix} \begin{bmatrix} d\sigma_{i-1} \\ d\sigma_i \\ d\sigma_{i+1} \end{bmatrix} + \begin{bmatrix} F_{1,i} & F_{2,i} \end{bmatrix} \begin{bmatrix} dh_{c,i} \\ d\dot{h}_{c,i} \end{bmatrix} + F_{5,i}\, dh_{\text{in},i}, \\ dh_{\text{out},i-1} = \begin{bmatrix} 1 & 0 \end{bmatrix} \begin{bmatrix} dh_{c,i-1} \\ d\dot{h}_{c,i-1} \end{bmatrix}. \end{cases} \tag{14}$$

For compactness, the two-bite process model can be rewritten by grouping the coefficient matrices as follows:

$$\begin{cases} \begin{bmatrix} \dot{\sigma}_{i-1} \\ \dot{\sigma}_i \\ \dot{\sigma}_{i+1} \end{bmatrix} = \mathbf{A}_{\text{pp},i-1:i} \begin{bmatrix} d\sigma_{i-1} \\ d\sigma_i \\ d\sigma_{i+1} \end{bmatrix} + \mathbf{B}_{\text{pp},i-1} \begin{bmatrix} dh_{c,i-1} \\ d\dot{h}_{c,i-1} \end{bmatrix} + \mathbf{B}_{\text{pp},i} \begin{bmatrix} dh_{c,i} \\ d\dot{h}_{c,i} \end{bmatrix} + \mathbf{G}_{\text{pp},i}\, dh_{\text{in},i}, \\ dF_{y,i-1} = \mathbf{C}_{\text{pp},i-1} \begin{bmatrix} d\sigma_{i-1} \\ d\sigma_i \\ d\sigma_{i+1} \end{bmatrix} + \mathbf{D}_{\text{pp},i-1} \begin{bmatrix} dh_{c,i-1} \\ d\dot{h}_{c,i-1} \end{bmatrix}, \\ dF_{y,i} = \mathbf{C}_{\text{pp},i} \begin{bmatrix} d\sigma_{i-1} \\ d\sigma_i \\ d\sigma_{i+1} \end{bmatrix} + \mathbf{D}_{\text{pp},i} \begin{bmatrix} dh_{c,i} \\ d\dot{h}_{c,i} \end{bmatrix} + L_{\text{pp},i}\, dh_{\text{in},i}, \\ dh_{\text{out},i-1} = \begin{bmatrix} 1 & 0 \end{bmatrix} \begin{bmatrix} dh_{c,i-1} \\ d\dot{h}_{c,i-1} \end{bmatrix} \end{cases} \tag{15}$$

The subscript pp is used to distinguish these matrices from the single-bite process matrices defined above. The structural models of the two neighboring stands presented in Eq. (12) can now be coupled with the two-bite process model in a manner analogous to that used to obtain Eq. (13). By substituting the structural outputs into the two-bite process model and by feeding the two rolling-force perturbations back into the corresponding structural models, the tension-coupled tandem model is obtained in Eq. (16):

$$\begin{cases} \begin{bmatrix} \dot{\mathbf{x}}_{s,i-1} \\ \dot{\mathbf{x}}_{s,i} \\ \dot{\sigma}_{i-1} \\ \dot{\sigma}_i \\ \dot{\sigma}_{i+1} \end{bmatrix} = \begin{bmatrix} \mathbf{A}_{s,i-1} + \mathbf{B}_{s,i-1}\mathbf{D}_{\text{pp},i-1}\mathbf{C}_{s,i-1} & \mathbf{0} & \mathbf{B}_{s,i-1}\mathbf{C}_{\text{pp},i-1} \\ \mathbf{0} & \mathbf{A}_{s,i} + \mathbf{B}_{s,i}\mathbf{D}_{\text{pp},i}\mathbf{C}_{s,i} & \mathbf{B}_{s,i}\mathbf{C}_{\text{pp},i} \\ \mathbf{B}_{\text{pp},i-1}\mathbf{C}_{s,i-1} & \mathbf{B}_{\text{pp},i}\mathbf{C}_{s,i} & \mathbf{A}_{\text{pp},i-1:i} \end{bmatrix} \begin{bmatrix} \mathbf{x}_{s,i-1} \\ \mathbf{x}_{s,i} \\ d\sigma_{i-1} \\ d\sigma_i \\ d\sigma_{i+1} \end{bmatrix} + \begin{bmatrix} \mathbf{0} \\ \mathbf{B}_{s,i}L_{\text{pp},i} \\ \mathbf{G}_{\text{pp},i} \end{bmatrix} dh_{\text{in},i}, \\ dh_{\text{out},i-1} = \begin{bmatrix} \begin{bmatrix} 1 & 0 \end{bmatrix} \mathbf{C}_{s,i-1} & \mathbf{0} & \mathbf{0} \end{bmatrix} \begin{bmatrix} \mathbf{x}_{s,i-1} \\ \mathbf{x}_{s,i} \\ d\sigma_{i-1} \\ d\sigma_i \\ d\sigma_{i+1} \end{bmatrix}. \end{cases} \tag{16}$$

which can be equivalently represented by the following single-input single-output (SISO) transfer function:

$$H(s) = \frac{dh_{\text{out},i-1}(s)}{dh_{\text{in},i}(s)} \tag{17}$$

Here, $H(s)$ denotes the instantaneous tension-mediated coupling between two neighboring stands, while its input and output are selected to describe the delayed regenerative path by which the exit-thickness perturbation $dh_{\text{out},i-1}$ is transported along the strip and becomes, after the delay Δ_i, the entry-thickness perturbation $dh_{\text{in},i}$ of the downstream stand; Hence, the autonomous form schematized in Fig. 4 would represent the complete internally delayed model of a tandem of two stands. This comprehensive model still displays negative damping on the single stands, with the only difference that now each stand has a dynamic boundary condition for the strip speed, dictated by the adjacent stand model. In this case, the phenomenon is addressed in literature as multi-stand negative damping effect [8,21]. But most importantly, through the strip transport effect, this model can also exhibit regenerative chatter. Marks generated by vibrations in the upstream stand travel with the strip and, after the transport delay Δ_i, enter the bite of the downstream stand. This

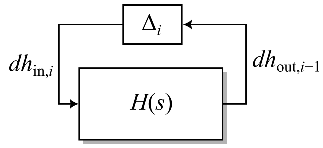

Figure 4 Autonomous two-stand regenerative chatter model. The block $H(s)$ represents the local two-stand transfer function from the entry-thickness perturbation of the downstream stand, $dh_{\mathrm{in},i}$, to the exit-thickness perturbation of the upstream stand, $dh_{\mathrm{out},i-1}$. The delay block Δ_i models the strip transport between stands: the thickness waviness generated at the exit of stand $i-1$ is convected with the strip and re-enters stand i after the transport time Δ_i, thereby closing the regenerative feedback loop.

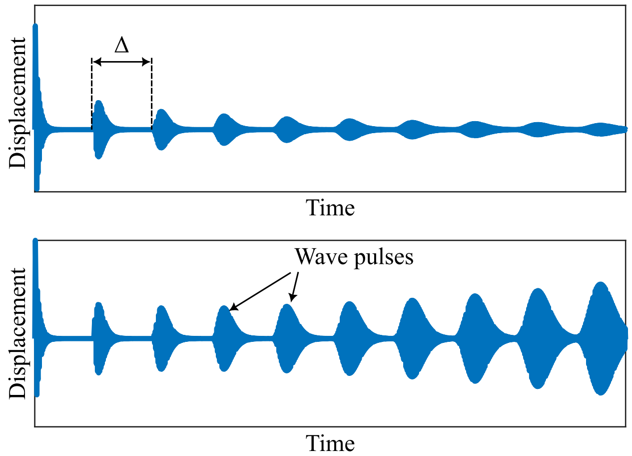

Figure 5 Qualitative schematic of the wavetrain behavior in regenerative vibrations. The top plot illustrates a stable case, where successive wave pulses separated by the transport delay Δ decrease in amplitude. The bottom plot illustrates an unstable case, where the wave pulses grow from one regenerative passage to the next.

interaction induces variations in the entry speed of the downstream stand and consequently alters the shared process state, which in turn excites further chattering in the upstream stand. Subsequently, new chatter marks are generated, and the process repeats; if each iteration displays greater vibration than the previous one, the pair of stands is unstable. The occurrence of regenerative chatter is readily identifiable by a wavetrain pattern exhibited in the mill vibration, as sketched in Fig. 5. This phenomenon is commonly referred to as modulation [21]. It is worth noting how the negative damping mechanism plays its role in the regenerative chatter by reducing the damping of vibrations in the individual stands.

3 Stability criterion

The multi-stand model of Fig. 4 is essentially an internally delayed system. Stability analysis of internally delayed systems has been the subject of numerous studies [22,23]. In particular, the work of Zhao and Ehmann [21] represents the first instance in which stability analysis in tandem rolling—specifically regarding the regenerative chatter mechanism—was investigated through the application of an integral criterion. However, while these methods provide rigorous tools for general internally delayed systems, the regenerative chatter mechanism as modeled here has a specific input–output structure that can be exploited to derive a simpler frequency-domain condition. In particular, the local two-stand model was reduced to a SISO transfer function whose input and output are the same physical quantity delayed in time. This formulation converts the regenerative chatter problem from the analysis of a general internally delayed multi-state system into the gain analysis of the loop composed of the local transfer function and the delay operator: $H(s)e^{-s\Delta_i}$.

This structure can be directly related to the small-gain theorem, which provides a sufficient stability condition for feedback interconnections in terms of the input–output gain of the open loop [24,25]. In the present SISO linear setting, this argument states that the delayed regenerative feedback is stable if the $\mathcal{H}_\infty$ norm of the open-loop regenerative gain is smaller than unity, namely

$$\left\|H(s)e^{-s\Delta_i}\right\|_\infty < 1. \tag{18}$$

For a SISO linear time-invariant system,

$$\left\|H(s)e^{-s\Delta_i}\right\|_\infty = \sup_\omega \left|H(\mathrm{j}\omega)e^{-\mathrm{j}\omega\Delta_i}\right|. \tag{19}$$

Since the delay operator has unit magnitude at every frequency:

$$\left|e^{-\mathrm{j}\omega\Delta_i}\right| = 1, \tag{20}$$

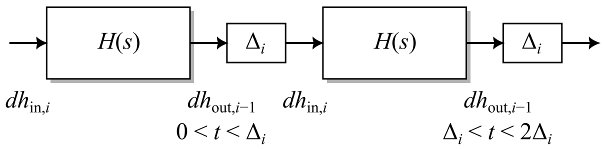

Figure 6 Pulse-by-pulse representation of the autonomous two-stand regenerative chatter model under the large-delay assumption. Starting from the closed-loop form of Fig. 4, the loop can be unfolded because consecutive perturbations are assumed not to overlap in time. Each block $H(s)$ represents one passage through the local two-stand model, while each delay Δ_i represents the strip transport time that maps the exit-thickness perturbation $dh_{\mathrm{out},i-1}$ into the next entry-thickness perturbation $dh_{\mathrm{in},i}$.

and it follows that

$$\left\| H(s)e^{-s\Delta_i} \right\|_\infty = \sup_\omega |H(\mathrm{j}\omega)| \,. \tag{21}$$

Therefore, the condition

$$\sup_\omega |H(\mathrm{j}\omega)| < 1 \tag{22}$$

is a robust sufficient stability condition for the regenerative loop. Conversely, the violation of Eq. (22) as an instability indicator is not, in general, an exact necessary and sufficient condition for arbitrary delayed feedback systems, since the phase of the loop also affects the location of the closed-loop characteristic roots.

Nevertheless, it will be shown that, under some operating conditions, the proposed magnitude-based criterion remains robust also as a sufficient condition for instability. Let us consider the extreme case in which Δ_i is sufficiently large for two consecutive system perturbations to remain independent in time, i.e., for their transient responses not to overlap. Hence, a large-delay condition is here intended as

$$\Delta_i \gg T_{\mathrm{sett}}, \tag{23}$$

where T_{sett} denotes the characteristic settling time of the coupled two-stand system. Physically, this means that the transport time required for a strip-thickness perturbation generated at the exit of stand $i-1$ to reach the entry of stand i is sufficiently long for the dynamic response caused by the previous perturbation to have essentially vanished. As qualitatively shown in Fig. 5, the initial part of the response may be approximated as a large-delay case, since consecutive wave pulses are sufficiently separated. , regarding the unstable case, as the regenerative mechanism amplifies the wave pulses, the effective settling time may become longer. Consequently, initially separated pulses can progressively overlap. The large-delay assumption should therefore be interpreted as a useful limiting case for deriving the pulse-amplification criterion, but not as a condition that remains necessarily valid throughout the entire unstable evolution.

Under this assumption, each wave pulse can be treated as independent regenerative passages as depicted in Fig. 6. The evolution of a harmonic component at angular frequency ω is obtained by evaluating the previous relation at $s = \mathrm{j}\omega$:

$$dh^{(k)}_{\mathrm{out},i-1}(\mathrm{j}\omega) = H(\mathrm{j}\omega)^k dh^{(0)}_{\mathrm{in},i}(\mathrm{j}\omega). \tag{24}$$

Taking the magnitude gives

$$\left| dh^{(k)}_{\mathrm{out},i-1}(\mathrm{j}\omega) \right| = |H(\mathrm{j}\omega)|^k \left| dh^{(0)}_{\mathrm{in},i}(\mathrm{j}\omega) \right|. \tag{25}$$

This expression shows that the amplitude of each frequency component is multiplied by $|H(\mathrm{j}\omega)|$ at every regenerative passage. Consequently, if there exists a frequency such that

$$|H(\mathrm{j}\omega)| > 1, \tag{26}$$

any initial perturbation containing a nonzero component at that frequency is amplified from one wave pulse to the next, therefore growing with k. The pair of stands $i-1$ and i is thus classified as susceptible to regenerative chatter. The effectiveness of this latter instability criterion when the large-delay hypothesis is relaxed will be examined in the next section.

4 Stability analysis

The two-stand case is here considered, using data from stands 4 and 5; For simplicity, parameters and results pertaining to stands 4 and 5 will henceforth be denoted with subscripts 1 and 2, respectively.

Performing a stability analysis in this context involves identifying the maximum operating speed—typically expressed as the peripheral speed of the work rolls in the last stand, $v_{\mathrm{r},2}$—at which the condition in Eq (22) is fullfilled for the two-stand tandem system. This threshold serves as a practical upper bound for safe operation and is particularly insightful when evaluated across a range of process and structural parameters, as it reveals the system's sensitivity to variations in those parameters and highlights regions of potential instability.

More specifically, for each selected combination of parameters the rolling speed of the downstream stand $v_{\mathrm{r},2}$ was progressively increased. For each imposed value of $v_{\mathrm{r},2}$, the upstream roll speed $v_{\mathrm{r},1}$ was computed iteratively from the nonlinear rolling-process model by enforcing inter-stand strip-speed continuity, namely $u_{\mathrm{out},1} = u_{\mathrm{in},2}$. At each point, the identified process parameters were substituted into the nonlinear rolling-process Eq. (1), and the process model was linearized about the corresponding steady operating

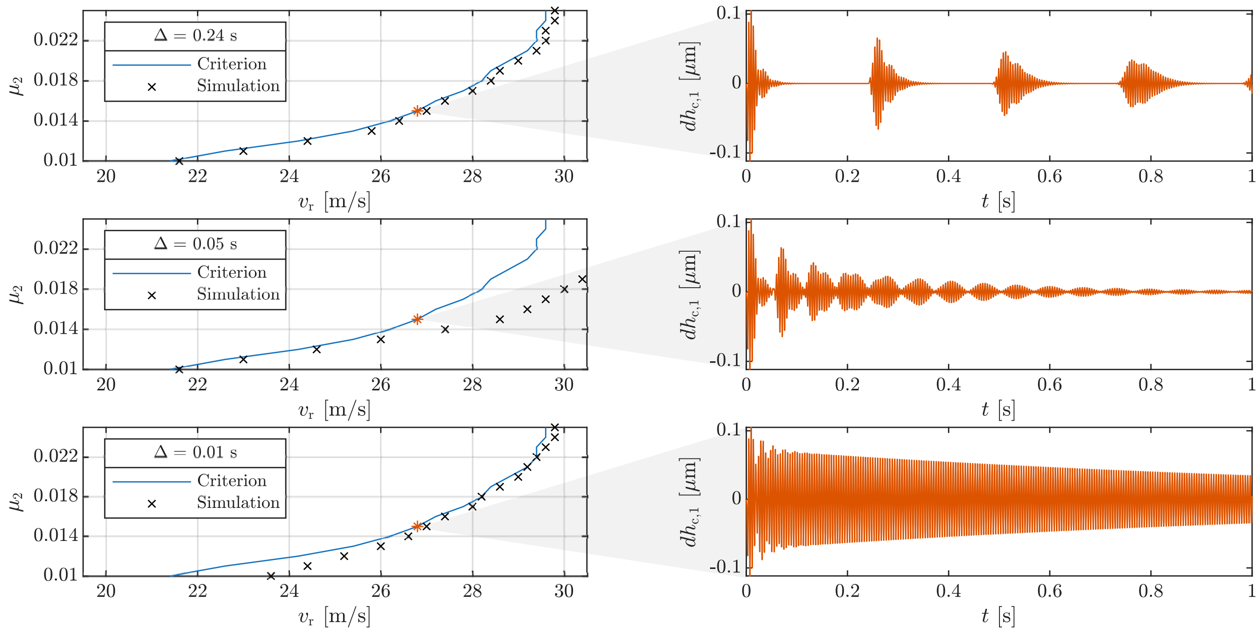

Figure 7 On the left: Comparison of the downstream friction μ_2 dependent stability margin computed with the proposed criterion against that evaluated through time simulations, for three different values of the delay term Δ. Critical speed values computed with the proposed criterion are linearly interpolated for visualization purposes. On the right: Visualization of the time simulation result at the working point denoted by the asterisk on the left plots.

point as in Eq. (2) to obtain the local coefficients $F_{1...5}$, $P_{1...5}$, and $Q_{1...5}$ for both stands. These coefficients were then used to assemble the local transfer function $H(s)$ for the selected operating condition as in Eqs. (16) and (17). The frequency response of $H(s)$ was then computed by discretizing the frequency interval 1–500 Hz with a frequency step of 1 Hz. More specifically, the transfer function was evaluated at the discrete frequencies $f = 1, 2, \ldots, 500$ Hz by substituting $s = \mathrm{j}2\pi f$. This interval was selected to cover the third-octave chatter range of the coupled stand–process system. In all investigated operating conditions, the maximum magnitude of $H(s)$ relevant to the proposed criterion was found in correspondence with this structural chatter mode, which lies within the selected frequency interval. According to the proposed criterion, the system was classified as certified stable when

$$\max_{f \in [1,500]\ \mathrm{Hz}} |H(\mathrm{j}2\pi f)| < 1. \tag{27}$$

For each set of paraemters, the target critical rolling speed $v_{r,2,crit}$ was therefore identified as the first value of $v_{r,2}$ for which Eq. (27) was no longer satisfied. After the first threshold crossing, all subsequent higher-speed points were checked to verify that the stability condition remained unsatisfied.

To obtain meaningful quantitative results, a specific model for both the process and structure must be selected together with an input data set. As anticipated in Section 1, the rolling process model employed herein is that one presented by Zhao and Ehmann [8,21] (the detailed derivation of which is provided in [26]). This allows for a better contextualization of this work with the state of the art for comparative purposes. The process parameters are the typical ones for a modern five-stand tandem rolling mill, as reported by Kimura et al. [27]. Two structural models are used, depending on the analysis purpose: a simplified vertical-symmetric single-degree-of-freedom (1-DOF) model and a more realistic vertical-symmetric 3-DOF model. The former is the one used by Zhao and Ehmann in [21], whereas details of the latter are reported in Appendix A.

4.1 Comparison against time-domain results. As a first step, it is essential to verify the effectiveness of the proposed stability criterion by comparing its predictions with results obtained from time-domain simulations. To this end, a stability analysis is conducted across a range of values for the downstream stand's strip-roll friction coefficient μ_2. This preliminary evaluation employs a simplified 1-DOF structural model. The choice of both the parameter to be swept and the simplified structural representation is intentional, as it mirrors the conditions used by Zhao and Ehmann in the validation of their integral criterion [21], thereby enabling a consistent and meaningful benchmark for comparison. Moreover, to test the criterion robustness when the large delay condition is not met, the study is repeated for several decreasing values of Δ. Keep in mind that the strip transport delay is inherently a function of the strip speed and the inter-stand length; varying Δ while disregarding these parameters is physically unrealistic.

4.1.1 Method. To verify the stability boundary predicted by the proposed frequency-domain criterion, an independent time-domain simulation was performed over the same parameter grid. The sweep was performed over $\mu_2 \in [0.010, 0.025]$ with a step of 0.001, while the downstream rolling speed was varied over $v_{r,2} \in [19, 31]$ m/s with a step of 0.2 m/s.

For each value of the downstream-stand friction coefficient μ_2, the critical speed was identified following the methodology illustrated in the introduction of Section 4.

Concerning time domain analysis, for each grid point the open-loop transfer function $H(s)$ was closed with a pure transport delay as

$$G_{cl}(s) = \frac{H(s)}{1 - H(s)e^{-s\Delta}}. \tag{28}$$

Three values of the transport delay were considered: $\Delta = 0.24$ s, 0.05 s, and 0.01 s. The first value corresponds to the delay computed from the nominal process data, whereas the latter two values were intentionally selected as artificially small delays to test the robustness of the criterion under increasingly severe regenerative-feedback conditions. The transfer function in Eq. (28) was simulated in MATLAB using the `lsim` command over $0 \le t \le 5$ s, with a uniformly sampled time vector and a sampling interval of $\Delta t = 1$ μs. The excitation was imposed as a finite-duration entry-thickness perturbation applied at the inlet of the downstream stand:

$$\delta h_{\text{in},2}(t) = \begin{cases} 10\ \mu\text{m}, & 0 \le t \le 0.1\ \text{ms}, \\ 0, & t > 0.1\ \text{ms}. \end{cases} \tag{29}$$

The monitored output was the roll-gap variation state $dh_{\text{c},1}$. Stability was assessed by comparing the response amplitude in two consecutive time windows at the end of the simulation. The peak amplitudes were defined as

$$A_{\text{last}} = \max_{5-2\Delta<t<5} \left| dh_{\text{c},1}(t) \right|, \qquad A_{\text{prev}} = \max_{5-4\Delta<t<5-2\Delta} \left| dh_{\text{c},1}(t) \right|. \tag{30}$$

The system was classified as unstable when

$$A_{\text{last}} > A_{\text{prev}} \quad \text{and} \quad A_{\text{prev}} > 10\ \text{nm}, \tag{31}$$

where the second condition avoids classifying numerical noise as a growing response. Otherwise, the simulated point was classified as stable.

The purpose of this comparison is not to use time-domain simulation as the primary stability tool, but to verify that the boundary predicted by the proposed frequency-domain criterion corresponds to the transition between decaying and growing delayed responses. The time-domain classification is therefore intentionally based on a simple growth criterion applied over the final delay periods of the simulation.

4.1.2 Results. The results of this analysis are reported on the left side of Fig. 7 (where the critical speeds computed with the proposed criterion were linearly interpolated for visualization purposes only). For all the tested delay values, no time-domain instability was observed below the stability limit predicted by the proposed criterion. This confirms the use of the criterion as a conservative stability condition: when the maximum frequency-response magnitude remains below unity, the delayed regenerative response is predicted to remain stable. The efficacy of the proposed criterion as an instability predictor is evident in the first case of large transport delay, because the criterion-based stability limit coincides with what was observed through time simulations. This delay value is the actual transport delay computed from the process parameters of the investigated case, rather than an artificial value, supporting the practical relevance of the large-delay interpretation in the present operating condition. Still, in the other cases of shorter delay, instability was not detected immediately above the formulated critical speeds. In fact, in some instances interactions between subsequent wave pulses (right side of Fig. 7) appeared to mitigate the regenerative effect even above the computed critical speed. Therefore, for short transport delays, exceeding the unity-gain threshold should be interpreted as the onset of a potentially unstable regenerative condition rather than as a sufficient indication of divergence in the time response. This observation might be misleading, as it could suggest that shorter delays improve stability. Nevertheless, as previously mentioned, the only means to decrease the transport delay in reality would be to increase the strip speed or reduce the inter-stand length, both of which would have an adverse effect on tandem stability [21].

These results clarify the role of the proposed criterion. In the general case, the criterion provides a sufficient condition for stability. Conversely, its use as a condition for instability is robust only when the strip transport delay is sufficiently large, i.e., when the delayed wave pulses are sufficiently separated so that they do not interact. The proposed stability margin is closely in agreement with the one formulated by Zhao and Ehmann through the integral criterion. A further advantage of the present approach lies in its computational efficiency. While Zhao and Ehmann report that the integral criterion may require up to a full day of computation on a 3 GHz CPU to map stability boundaries over a fine parameter grid [21], the present method only involves the evaluation of a linear frequency response function and can therefore be executed within minutes.

4.2 Friction effect on stability. Chatter is closely related to friction conditions in roll bites. However, its influence is not yet clearly understood, and the conclusions reached in the literature are sometimes contradictory [27]. In this section, a stability analysis of regenerative chatter with respect to friction conditions of both upstream and downstream stand is conducted, and an attempt is made to elucidate these discrepancies. To obtain more meaningful results, the more realistic 3-DOF structural model is employed.

4.2.1 Method. As discussed in Section 2, variations in process parameters affect the stand dynamics via model matching and negative damping. In other words, friction variations influence stability directly through the negative-damping effect and indirectly by altering the stand-chattering frequency, as schematically illustrated in Fig. 8. To isolate the direct effect of friction, the model matching effect can be eliminated by assigning a fixed value to F_1, while all other coefficients are kept dependent on the process parameters. Since F_1 represents the rolling-contact stiffness contribution, fixing this coefficient prevents the friction-dependent shift of the stand chatter frequency, while preserving the dependence of the process damping, tension coupling, and velocity perturbation terms on the operating point. This maintains a constant stand-chattering frequency. In the fixed-frequency case, the value of F_1 was therefore kept equal to its nominal value, whereas the remaining process coefficients F_2–F_5, P_1–P_5, and Q_1–Q_5 were updated at each point of the parameter grid. The same analysis was also repeated in nominal conditions, i.e., with all process coefficients recomputed as functions of the local friction and speed values.

The stability map was computed on a two-dimensional grid of upstream and downstream friction coefficients. The upstream friction coefficient μ_1 was varied in the range $[0.012, 0.028]$, while the downstream friction coefficient μ_2 was varied in the range $[0.010, 0.022]$, both with a step of 5×10^{-4}. These intervals were selected as neighborhoods of the corresponding nominal operating friction values. For each pair (μ_1, μ_2), the downstream rolling speed $v_{\text{r},2}$ was swept from 15 to 40 m/s with a step of 0.1 m/s.

At each point of the parameter grid, the critical speed was identified following the methodology illustrated in the introduction of Section 4. The resulting value of $v_{\text{r},2,\text{crit}}$ was then stored and plotted over the (μ_1, μ_2) plane. For visualization purposes only, the stored values of $v_{\text{r},2,\text{crit}}$ were rendered as a continuous surface using MATLAB `surface` with a linearly interpolated face coloring. The contour lines were obtained from the same discrete grid. No interpolation was used to determine the critical speeds, which were extracted directly from the discrete parameter sweep.

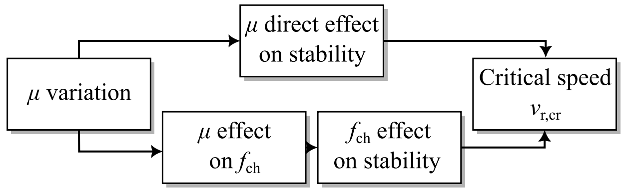

Figure 8 Friction effect on stability through negative-damping (top path) and model-matching (bottom path).

4.2.2 Results. Stability charts presented in Fig. 9 and 10, respectively, depict the friction effect on stability without and with the model matching effect. Through several simulations performed on different models, it is observed that the behavior depicted in Fig. 9 tends to be more consistent across cases, whereas the overall effect shown in Fig. 10 varies from one case to another. This variability is likely due to the sensitivity of the chatter frequency to process stiffness, which strongly depends on the adopted structural model. From an engineering point of view, this means that the direct negative-damping contribution of friction is relatively robust, whereas the indirect contribution associated with frequency shifting is model-dependent. It is evident for example that the impact of the process stiffness variation on the dynamics of a simple 1-DOF structural model differs markedly from that of a more realistic higher-order model. Therefore, although oversimplified models offer ease of analysis for chatter studies, they should be used with caution. They may correctly reproduce the qualitative destabilizing role of process damping, but they can distort the stabilizing or destabilizing effect associated with the displacement of the chatter mode through model matching.

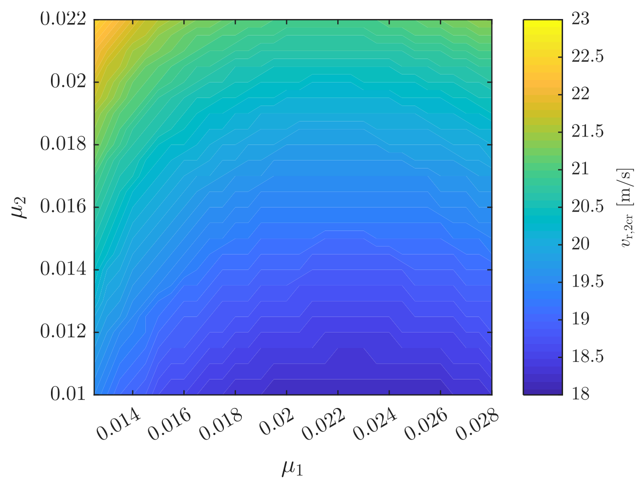

Figure 9 Upstream (μ_1) and downstream (μ_2) friction coefficient effect on the critical rolling speed of the stand pair through negative-damping only (fixed chatter frequency).

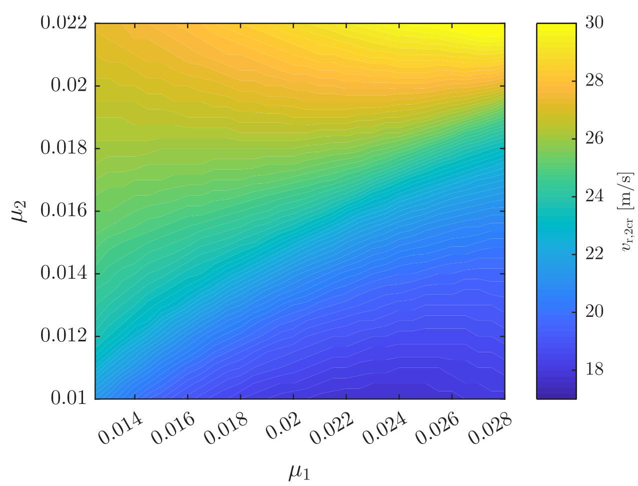

Figure 10 Upstream (μ_1) and downstream (μ_2) overall friction coefficient effect on the critical rolling speed of the stand pair.

The chart in Fig. 9 can be discussed in greater detail. For a fixed structural dynamic, the stand pair appears to be monotonically more stable with higher friction in the downstream stand, while a critical friction condition is observed in the upstream stand. This asymmetric behavior is a direct consequence of the different roles played by the two stands in the regenerative loop: the downstream stand receives the transported thickness perturbation, whereas the upstream stand is responsible for generating the exit waviness that closes the feedback path after transport. The rationale behind this behavior is that, under lower friction conditions, an individual stand is known to be more susceptible to negative damping. However, in the upstream stand 1, although low friction enhances self-excited chatter, it simultaneously reduces the stand's receptivity to exit inter-stand stress variations, which are critical for the regenerative mechanism. In other words, the friction coefficient does not only change the local tendency of the stand to self-excite; it also changes how efficiently perturbations are transmitted through the inter-stand tension and converted into new thickness waviness. This phenomenon explains the increased regenerative chatter stability observed for low friction in stand 1 and the emergence of a critical friction condition. The resulting stability boundary should therefore not be interpreted as a simple monotonic effect of friction on local chatter tendency, but as the outcome of two competing mechanisms: local negative-damping amplification and regenerative coupling efficiency.

4.3 Structure dynamic effect on stability. The chatter frequency of a stand, f_{ch}, i.e., the frequency at which self-excited vibration occurs, plays a central role in determining system stability in both single- and multi-stand configurations. In this work, f_{ch} is defined as the resonance frequency of the locally coupled stand–process system, namely the structural dynamics of the stand including the rolling-contact stiffness contribution associated with F_1. Therefore, it should not be interpreted as the free natural frequency of the stand alone, but as the effective resonance frequency after the process stiffness has been included. While it is partially influenced by the strip-roll contact stiffness (model matching effect, as discussed in Section 2), it is predominantly governed by the dynamic properties of the mill structure and thus emerges as a direct consequence of mill design. In the case of single-stand chatter, a common design recommendation is to maximize vertical stiffness to shift the natural frequencies away from instability-prone regions. However, when it comes to tandem rolling, systematic design guidelines to enhance multi-stand stability—particularly in relation to inter-stand dynamic coupling—remain largely undeveloped.

In the following, a parametric stability analysis is carried out for a pair of coupled stands in the plane defined by the upstream and downstream stand chatter frequencies ($f_{\mathrm{ch},1}$ and $f_{\mathrm{ch},2}$), with the goal of identifying favorable design regions and clarifying how relative frequency placement can be leveraged to mitigate regenerative chatter.

4.3.1 Method. As in the previous analyses, the critical strip speed is computed for each point in the parameter space. In this case, all process-related parameters, except for the strip speed, are held constant at the nominal operating condition. The purpose of the analysis is to isolate the influence of the relative placement of the upstream and downstream stand chatter frequencies on the regenerative stability limit.

The two-dimensional parameter space is defined by the chatter frequencies of the upstream and downstream stands, denoted as $f_{\mathrm{ch},1}$ and $f_{\mathrm{ch},2}$, respectively. Both frequencies were varied in the range 150–250 Hz with a step of 2.5 Hz. These frequency variations were introduced by scaling the mass matrix of the structural model through the scalar gain g_{m}, as described in Appendix A.

At each frequency pair $(f_{\mathrm{ch},1}, f_{\mathrm{ch},2})$, the critical speed was identified following the methodology illustrated at the beginning of Section 4.

The resulting value was stored and plotted over the $(f_{\mathrm{ch},1}, f_{\mathrm{ch},2})$ plane. For visualization purposes only, the stored values of $v_{\mathrm{r},2,\mathrm{crit}}$ were rendered as a continuous surface using MATLAB `surface` with linearly interpolated face coloring. The contour lines were obtained from the same discrete grid. No interpolation was used to determine the critical speeds, which were extracted directly from the discrete parameter sweep.

4.3.2 Results. Results are presented in Fig. 11. This study confirms that the system exhibits greater stability at higher chatter frequencies, a phenomenon attributed to the negative damping effect being more pronounced at lower frequencies. From a physical standpoint, lower chatter frequencies correspond to longer vibration periods, allowing larger inter-stand stress perturbations to build up from the velocity mismatch induced by the roll-gap oscillation. As a result, the process-related force component that feeds energy into the vibration becomes more effective at low frequencies. Nonetheless, it is of more interest to examine the impact of a relative variation in chatter frequency between the two stands. Two optimal zones are identified; they can be attributed to the decoupling of resonance peaks within the stand pair. Specifically, starting from any point along the diagonal (same frequency condition), a decrease in a stand's resonant frequency results in an enhanced negative damping effect, although the beneficial impact of resonance peak decoupling is most pronounced at the onset of this variation. This indicates that the first-order benefit does not come from simply lowering or increasing one chatter frequency, but from preventing the two stands from responding strongly at the same frequency. In engineering terms, two identical or nearly identical stands behave as efficient receivers and transmitters of the same disturbance, whereas a frequency mismatch weakens this regenerative exchange.

However, it is apparent that the upper-left optimal zone where $f_{\mathrm{ch},2} < f_{\mathrm{ch},1}$ yields higher critical speeds compared to the lower-right zone where $f_{\mathrm{ch},2} > f_{\mathrm{ch},1}$. This behavior is due to the presence of an anti-resonance in the system that relates process forces on the work rolls to chatter vibrations. This anti-resonance consistently occurs closely above the resonant frequency [28]. If the resonant frequency of stand 2 coincides with the anti-resonance of stand 1, a significant mitigation of regenerative chatter can be achieved, as the chatter marks exiting stand 1 are directly generated by the chatter in that stand. In this configuration, the downstream stand tends to excite the upstream stand at a frequency for which the upstream force-to-gap response is locally minimized. The thickness waviness generated at the exit of the upstream stand is therefore reduced, weakening the delayed feedback path that sustains the regenerative mechanism. Notably, this phenomenon is not reciprocal i.e., when the resonance of stand 1 overlaps the anti-resonance of stand 2. Specifically, the entry strip thickness variation in stand 2 can directly induce inter-stand stress vibrations without the mediation of chatter vibrations. Thus, the anti-resonance of the downstream stand does not attenuate the same physical quantity in the same position of the feedback loop. This explains why the two off-diagonal stability regions are not symmetric, even though they both arise from a relative shift between the two structural chatter frequencies.

The key finding of this analysis is that avoiding identical mill structures can be advantageous in mitigating regenerative chatter. A comparison with the analogous regenerative effect encountered in metal-cutting machines further supports this observation. While in turning machines the marks created by a system re-enter the same system, in a rolling mill the marks generated by a stand do not re-enter the same stand. Still, they re-enter an identical one, thereby transmitting vibrations via inter-stand tension. Consequently, it is reasonable to assume that stands with differing characteristics will not interact in the same manner as two identical stands, thereby potentially inhibiting resonant behavior. The practical implication is that structural tuning should not aim only at shifting all stand modes to higher frequencies. A deliberate detuning between neighboring stands, especially when the downstream resonance is placed close to

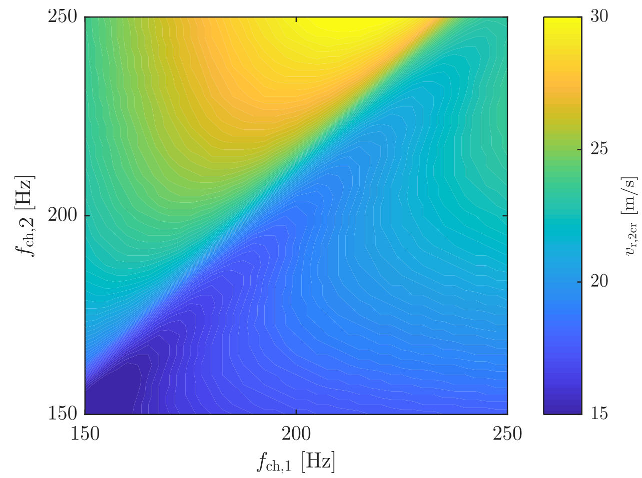

Figure 11 Upstream ($f_{\mathrm{ch},1}$) and downstream ($f_{\mathrm{ch},2}$) stand-chattering frequency effect on the critical rolling speed of the stand pair.

the upstream anti-resonance, can be more effective in reducing the regenerative loop gain. This result also highlights why conclusions drawn from overly simplified structural models should be treated carefully: if the model does not reproduce the relevant anti-resonance pattern, it may miss the most favorable tuning condition.

5 Conclusions

This work has presented a novel stability criterion for regenerative chatter in tandem cold rolling mills, addressing one of the primary bottlenecks in cold rolling productivity. By leveraging linear analysis tools, this approach provides an efficient and precise alternative to the state-of-the-art integral method. The proposed formulation recasts the regenerative mechanism as a delayed SISO feedback loop, where the local two-stand transfer function is coupled with the strip-transport delay. Within this framework, the criterion provides a robust sufficient condition for stability, consistently with a small-gain-type interpretation. Its use as an instability indicator is instead justified by the pulse-amplification interpretation and becomes particularly reliable when the strip transport delay is sufficiently large for successive wave pulses to remain well separated. The criterion is designed for general applicability and was validated against the state-of-the-art benchmark model and corresponding data for a modern five-stand tandem rolling mill. Time-domain simulations confirmed that the proposed stability criterion is effective, particularly when the strip transport delay is sufficiently large. Therefore, the criterion should be interpreted primarily as a certified-stability condition, while the loss of this condition identifies operating points that are potentially susceptible to regenerative instability. Under large-delay conditions, this susceptibility closely corresponds to the actual onset of regenerative chatter observed in time-domain simulations.

The proposed criterion has been employed to generate multi-parametric stability charts that not only validate its effectiveness but also shed light on inconsistencies reported in previous studies, where it was observed how different assumptions on the structural model can lead to very different results for parametric stability analysis for the regenerative case. Notably, such evaluations could be completed in a matter of minutes, compared to the full-day computational times reported by previous works without any loss in the accuracy of instability prediction. This computational advantage makes the method suitable for repeated parameter sweeps and preliminary design studies, where the objective is not only to verify a single operating condition but also to understand how stability margins evolve with process and structural parameters.

Furthermore, a parametrization strategy was introduced to investigate the impact of structural modifications in the stands and to identify favorable design configurations capable of mitigating regenerative chatter. The analysis revealed that aligning the resonance of the downstream stand with the anti-resonance of the upstream stand can significantly improve the stability of the system for the regenerative case. This result suggests that regenerative chatter mitigation should not be pursued only by increasing the natural frequencies of individual stands, but also by deliberately tuning the relative dynamic placement of neighboring stands. In particular, structural detuning can reduce the effectiveness of the delayed feedback path by weakening the transmission of chatter-induced thickness waviness from one stand to the next.

Future works will focus on exploiting these insights to develop targeted strategies for monitoring and reducing regenerative chatter in cold rolling operations, ultimately leading to improved process stability and productivity.

Nomenclature

i = stand index
k = wave-pulse index
t = time
s = Laplace variable
j = imaginary unit
f = frequency
ω = angular frequency
$d(\cdot)$ = small perturbation around the steady operating condition
h_{c} = roll-gap height
$\dot{h}_{\mathrm{c}}$ = roll-gap height rate of change
h_{in} = entry strip thickness

h_{out} = exit strip thickness/chatter mark
u_{in} = entry strip speed
u_{out} = exit strip speed
v_{r} = work-roll peripheral velocity
$v_{\mathrm{r,crit}}$ = critical work-roll peripheral velocity for regenerative chatter
F_{y} = vertical rolling force
σ = inter-stand strip stress
μ = friction coefficient between strip and roll
$\mathbf{p}_{\mathrm{mat}}$ = material-parameter vector of the selected rolling law
R = work-roll radius
E = rolled material Young's modulus
L_i = distance between stands $i-1$ and i
Δ_i = strip transport time delay between stands $i-1$ and i
T_{sett} = characteristic settling time of the two-stand tandem system
f_{ch} = coupled stand–process chatter frequency
$P_1, \ldots, P_5$ = linearized sensitivities of entry strip speed
$Q_1, \ldots, Q_5$ = linearized sensitivities of exit strip speed
$F_1, \ldots, F_5$ = linearized sensitivities of vertical rolling force
$\mathbf{\Phi}$ = generic nonlinear rolling-bite process function
$H(s)$ = local SISO transfer function of the two-stand tandem between entry- and exit-thickness perturbations
$G_{\mathrm{cl}}(s)$ = closed-loop delayed regenerative transfer function
$\delta h_{\mathrm{in},2}$ = entry-thickness perturbation applied to the downstream stand for time-domain simulation
$A_{\mathrm{last}}, A_{\mathrm{prev}}$ = peak response amplitudes in the last and preceding time windows of the time-domain simulation
$\mathbf{x}_{\mathrm{s}}$ = structural state vector
$\mathbf{A}, \mathbf{B}, \mathbf{C}, \mathbf{D}$ = generic state-space matrices
$\mathbf{A}_{\mathrm{s}}, \mathbf{B}_{\mathrm{s}}, \mathbf{C}_{\mathrm{s}}$ = structural state-space matrices
$\mathbf{A}_{\mathrm{p}}, \mathbf{B}_{\mathrm{p}}, \mathbf{C}_{\mathrm{p}}, \mathbf{D}_{\mathrm{p}}, \mathbf{G}_{\mathrm{p}}, \mathbf{L}_{\mathrm{p}}$ = single-bite process state-space matrices
$\mathbf{A}_{\mathrm{pp}}, \mathbf{B}_{\mathrm{pp}}, \mathbf{C}_{\mathrm{pp}}, \mathbf{D}_{\mathrm{pp}}, \mathbf{G}_{\mathrm{pp}}, \mathbf{L}_{\mathrm{pp}}$ = two-bite process state-space matrices
g_{m} = structural mass scaling factor
$(\cdot)^{(k)}$ = quantity associated with the kth regenerative passage
$(\cdot)_{\mathrm{op}}$ = quantity evaluated at operating point op
$\|\cdot\|_\infty$ = $\mathcal{H}_\infty$ norm

Appendix A: 3-DOF structure model

The more realistic vertical-symmetric 3-DOF structural model, representing a six-high mill stand, is schematized in Fig. 12. Its lumped mass and stiffness parameters are listed in Table 1. Such parameter values are commonly used in the literature for similar models. It is worth noting that the numerical accuracy of the structural model is not critical for the purposes of this paper. The mass and stiffness matrices are reported in Eqs. (A1) and (A2) where the gain g_{m} is used to modulate the stand resonant chatter frequency. The damping matrix is modeled via the modal damping technique, considering a damping ratio of 0.005.

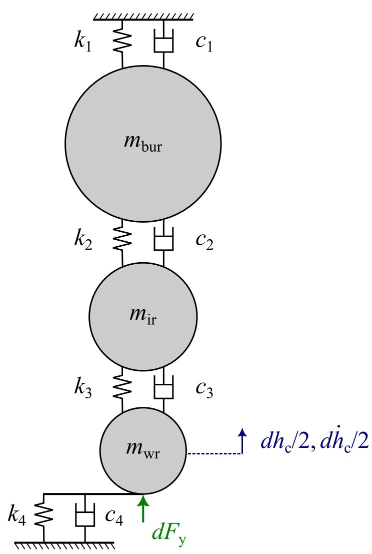

Figure 12 Scheme of the vertical-symmetric 3-DOF model of a six-high mill rolling stand

$$M = \begin{bmatrix} m_{\mathrm{bur}} & 0 & 0 \\ 0 & m_{\mathrm{ir}} & 0 \\ 0 & 0 & m_{\mathrm{wr}} \end{bmatrix} g_{\mathrm{m}} \tag{A1}$$

Table 1 Mechanical parameters of the rolling system

Parameter	Value	Unit
k_1	69	MN/m
k_2	121.44	MN/m
k_3	135.7	MN/m
k_4	14.5	MN/m
m_{bur}	$60 \cdot 10^3$	kg
m_{ir}	$9.2 \cdot 10^3$	kg
m_{wr}	$8.3 \cdot 10^3$	kg

$$K = \begin{bmatrix} k_1 + k_2 & -k_2 & 0 \\ -k_2 & k_2 + k_3 & -k_3 \\ 0 & -k_3 & k_3 + k_4 \end{bmatrix} \tag{A2}$$

References

[1] Tamiya, T., Furui, K., and Iida, H., 1980, "Analysis of chattering phenomenon in cold rolling," *International Conference on Steel Rolling,*, Vol. 2, Tokyo, Japan, Sep. 1980, pp. 1191–1202.
[2] Tlusty, J., Chandra, G., Critchley, S., and Paton, D., 1982, "Chatter in Cold Rolling," CIRP Annals, **31**(1), pp. 195–199.
[3] Wilson, W. R. D., 1997, "Tribology in Cold Metal Forming," Journal of Manufacturing Science and Engineering, **119**(4B), pp. 695–698.
[4] Yun, I., Wilson, W., and Ehmann, K., 1998, "Review of chatter studies in cold rolling," International Journal of Machine Tools and Manufacture, **38**(12), pp. 1499–1530.
[5] Hu, P.-H., Zhao, H., and Ehmann, K. F., 2006, "Third-octave-mode chatter in rolling. Part 1: Chatter model," Proceedings of the Institution of Mechanical Engineers, Part B: Journal of Engineering Manufacture, **220**(8), pp. 1267–1277.
[6] Hu, P.-H., Zhao, H., and Ehmann, K. F., 2006, "Third-octave-mode chatter in rolling. Part 2: Stability of a single-stand mill," Proceedings of the Institution of Mechanical Engineers, Part B: Journal of Engineering Manufacture, **220**(8), pp. 1279–1292.
[7] Hu, P.-H., Zhao, H., and Ehmann, K., 2006, "Third-octave-mode chatter in rolling. Part 3: stability of a multi-stand mill," Proceedings of the Institution of Mechanical Engineers, Part B: Journal of Engineering Manufacture, **220**(8), pp. 1293–1303.
[8] Zhao, H. and Ehmann, K. F., 2013, "Stability Analysis of Chatter in Tandem Rolling Mills—Part 1: Single- and Multi-Stand Negative Damping Effect," Journal of Manufacturing Science and Engineering, **135**(3), p. 031001.
[9] Yun, I.-S., Wilson, W. R. D., and Ehmann, K. F., 1998, "Chatter in the Strip Rolling Process, Part 1: Dynamic Model of Rolling," Journal of Manufacturing Science and Engineering, **120**(2), pp. 330–336.
[10] Yun, I.-S., Ehmann, K. F., and Wilson, W. R. D., 1998, "Chatter in the Strip Rolling Process, Part 2: Dynamic Rolling Experiments," Journal of Manufacturing Science and Engineering, **120**(2), pp. 337–342.
[11] Meehan, P. A., 2002, "Vibration instability in rolling mills: modeling and experimental results," J. Vib. Acoust., **124**(2), pp. 221–228.
[12] Hu, P.-H., 1998, *Stability and chatter in rolling*, Northwestern University.
[13] Yun, I.-S., 1995, *Chatter in rolling*, Northwestern University.
[14] Yun, I.-S., Ehmann, K. F., and Wilson, W. R. D., 1998, "Chatter in the Strip Rolling Process, Part 3: Chatter Model," Journal of Manufacturing Science and Engineering, **120**(2), pp. 343–348.
[15] Hu, P.-H. and Ehmann, K. F., 2000, "A dynamic model of the rolling process. Part I: homogeneous model," International Journal of Machine Tools and Manufacture, **40**(1), pp. 1–19.
[16] Niroomand, M. R., Forouzan, M., Salimi, M., and Kafil, M., 2012, "Frequency analysis of chatter vibrations in tandem rolling mills," Journal of Vibroengineering, **14**, pp. 852–865.
[17] Chefneux, L., Fischbach, J.-P., and Gouzou, J., 1984, "Study and industrial control of chatter in cold rolling," Iron and Steel Engineer, **61**(11), pp. 17–26.
[18] Niroomand, M. R., Forouzan, M., Salimi, M., and Shojaei, H., 2012, "Experimental Investigations and ALE Finite Element Method Analysis of Chatter in Cold Strip Rolling," ISIJ International, **52**, pp. 2245–2253.
[19] Niroomand, M. R., Forouzan, M., and Salimi, M., 2015, "Theoretical and Experimental Analysis of Chatter in Tandem Cold Rolling Mills Based on Wave Propagation Theory," ISIJ International, **55**, pp. 637–646.
[20] Niroomand, M. R., Forouzan, M., and Heidari, A., 2018, "Experimental Analysis of Vibration and Sound in Order to Investigate Chatter Phenomenon in Cold Strip Rolling," International Journal of Advanced Manufacturing Technology, **100**, pp. 673–682.
[21] Zhao, H. and Ehmann, K. F., 2013, "Stability Analysis of Chatter in Tandem Rolling Mills—Part 2: The Regenerative Effect," Journal of Manufacturing Science and Engineering, **135**(3), p. 031002.
[22] Drozdov, A. D. and Kolmanovskii, V. B., 1994, "Chapter 7 - Stability of Functional Differential Equations," *Stability in Viscoelasticity*, Vol. 38 of North-Holland Series in Applied Mathematics and Mechanics, North-Holland, pp. 501–549.
[23] Stépán, G., 1989, *Retarded dynamical systems : stability and characteristic functions / G. Stépán*, Pitman research notes in mathematics series, Longman, Harlow.
[24] Zames, G., 1966, "On the Input-Output Stability of Time-Varying Nonlinear Feedback Systems Part One: Conditions Derived Using Concepts of Loop Gain, Conicity, and Positivity," IEEE Transactions on Automatic Control, **11**(2), pp. 228–238.
[25] Zhou, K., Doyle, J. C., and Glover, K., 1996, *Robust and Optimal Control*, Prentice Hall.
[26] Zhao, H., 2008, "Regenerative chatter in cold rolling," .
[27] Kimura, Y., Sodani, Y., Nishiura, N., Ikeuchi, N., and Mihara, Y., 2003, "Analysis of Chatter in Tandem Cold Rolling Mills," ISIJ International, **43**(1), pp. 77–84.
[28] Valigi, M. C., Cervo, S., and Petrucci, A., 2014, "Chatter Marks and Vibration Analysis in a S6-High Cold Rolling Mill," *Advances in Condition Monitoring of Machinery in Non-Stationary Operations*, G. Dalpiaz, R. Rubini, G. D'Elia, M. Cocconcelli, F. Chaari, R. Zimroz, W. Bartelmus, and M. Haddar, eds., Springer, Ferrara, Italy, May 2013, pp. 567–575.